

Supporting Information

for

**Cooperative adsorption performance of topological nodal surface
fermions and excess electrons in three-dimensional topological
electride Ba_3CrN_3**

Zhizuo Liu^a, Ying Liu^{*a}, Zihan Li^a, Xuefang Dai^a, Xiaoming Zhang^{*a}, and Guodong
Liu^{*a}

^a. State Key Laboratory of Reliability and Intelligence of Electrical Equipment, and
School of Materials Science and Engineering, Hebei University of Technology, Tianjin,
300130, China

Supplementary Figures

The band structures of Ba_3CrN_3 with different U values are calculated, as shown in Fig. S1. The nodal surface is always stable under different U values.

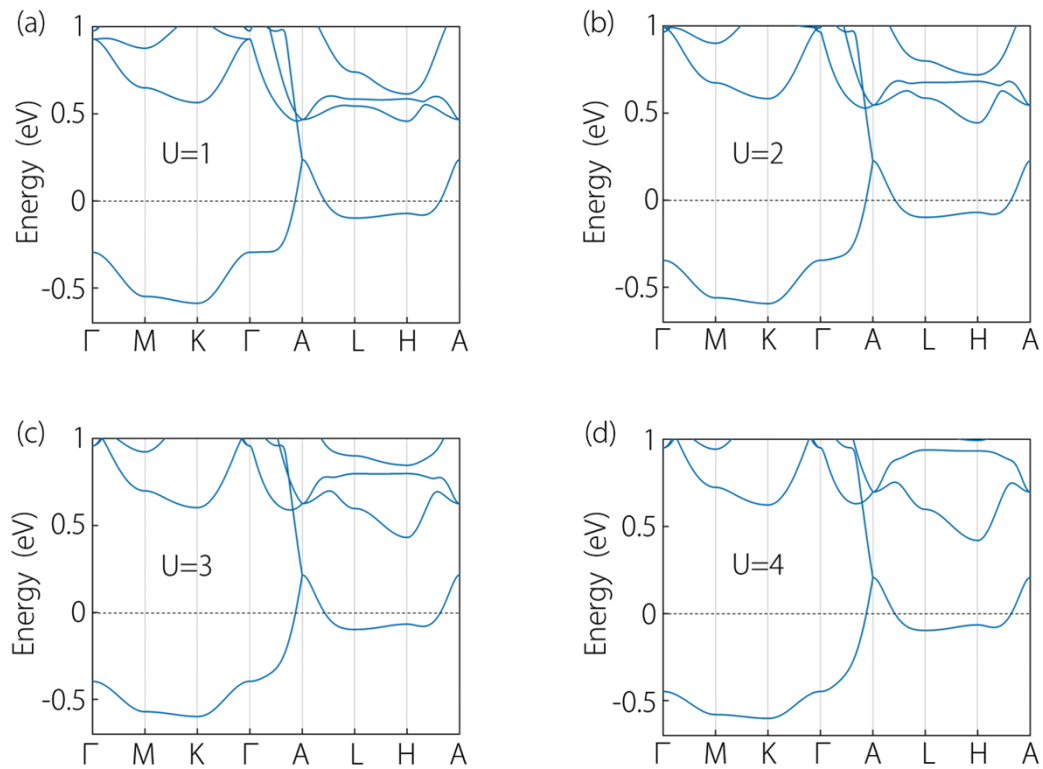


Fig. S1 The band structure of Ba_3CrN_3 with (a) $U=1$ eV, (b) $U=2$ eV, (c) $U=3$ eV and (d) $U=4$ eV.

We calculated the surface states of Ba_3CrN_3 's (100) surface without/with SOC, as shown in Fig. S2. There are obvious Fermi arcs on the (100) surface without SOC, which are labeled by the arrows in Fig. S2a. As shown in Fig. S2b, it is observed that the Fermi arcs still exist and splits into two arcs due to the spin-splitting bands.

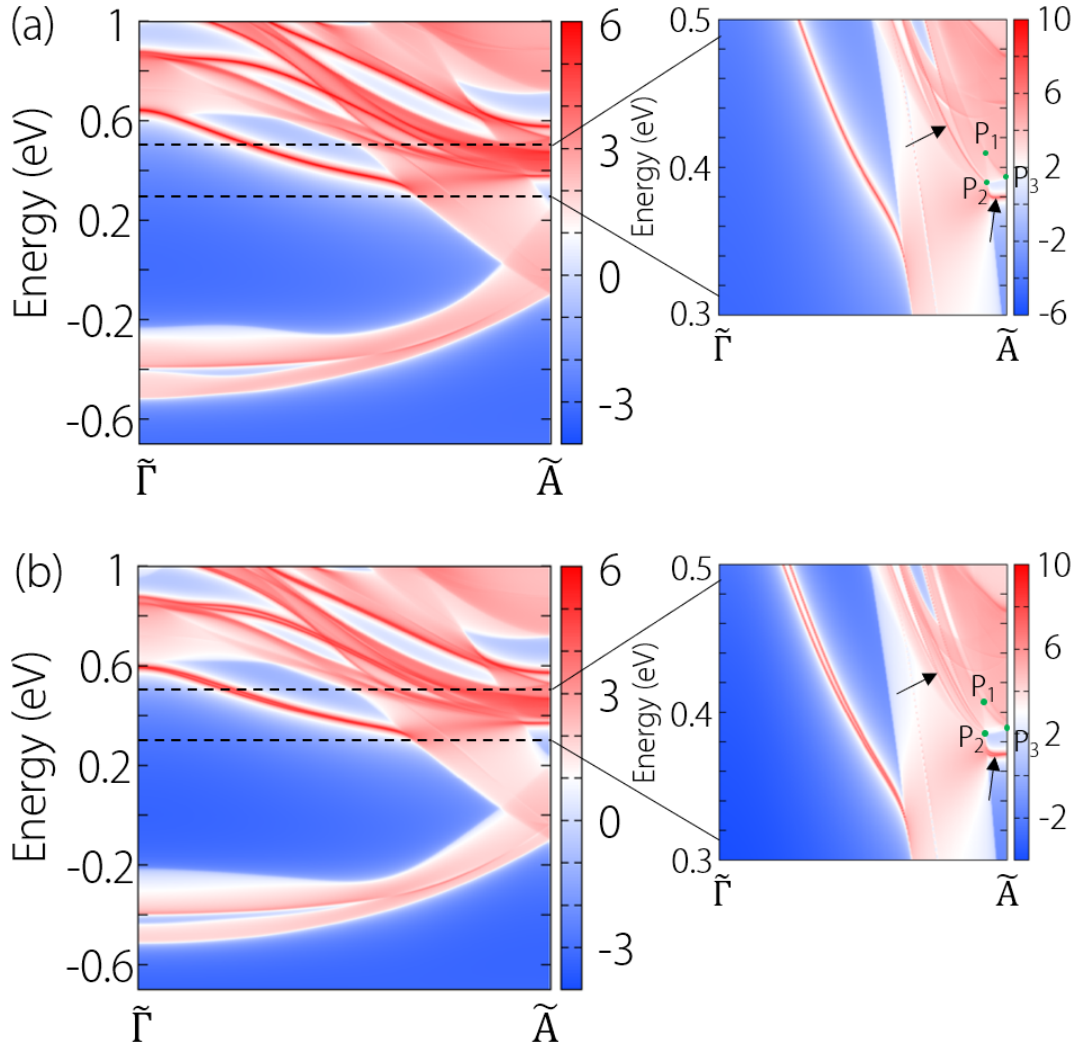


Fig. S2 Surface states (a) without SOC and (b) with SOC for Ba_3CrN_3 's (100) surface. The illustration on the right is an enlargement of the dotted range of the image on the left. The green points are the positions of the band crossings, and the arrows point to the Fermi arcs states.

The SOC effect in Ba_3CrN_3 is studied as shown in Fig. S3. P_1 , P_2 and P_3 open the SOC energy gap of 16 meV, 5 meV and 4 meV, respectively and a new Weyl point P_4 forms. On the A-L-H-A path, the nodal surface opens a maximum energy gap of only 28 meV at H and form a new Weyl point P_5 at L.

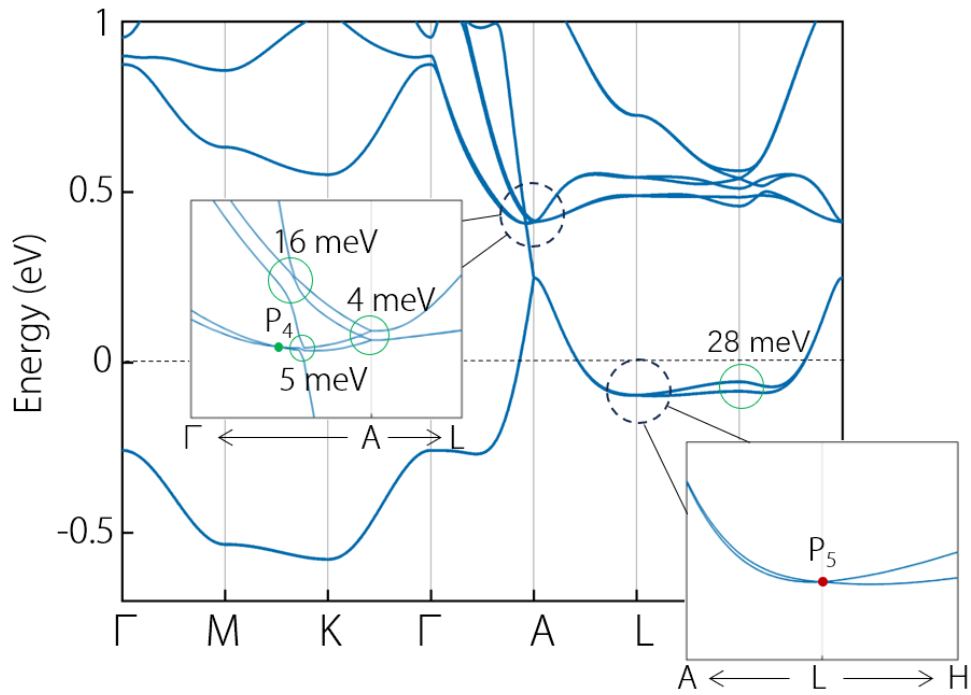
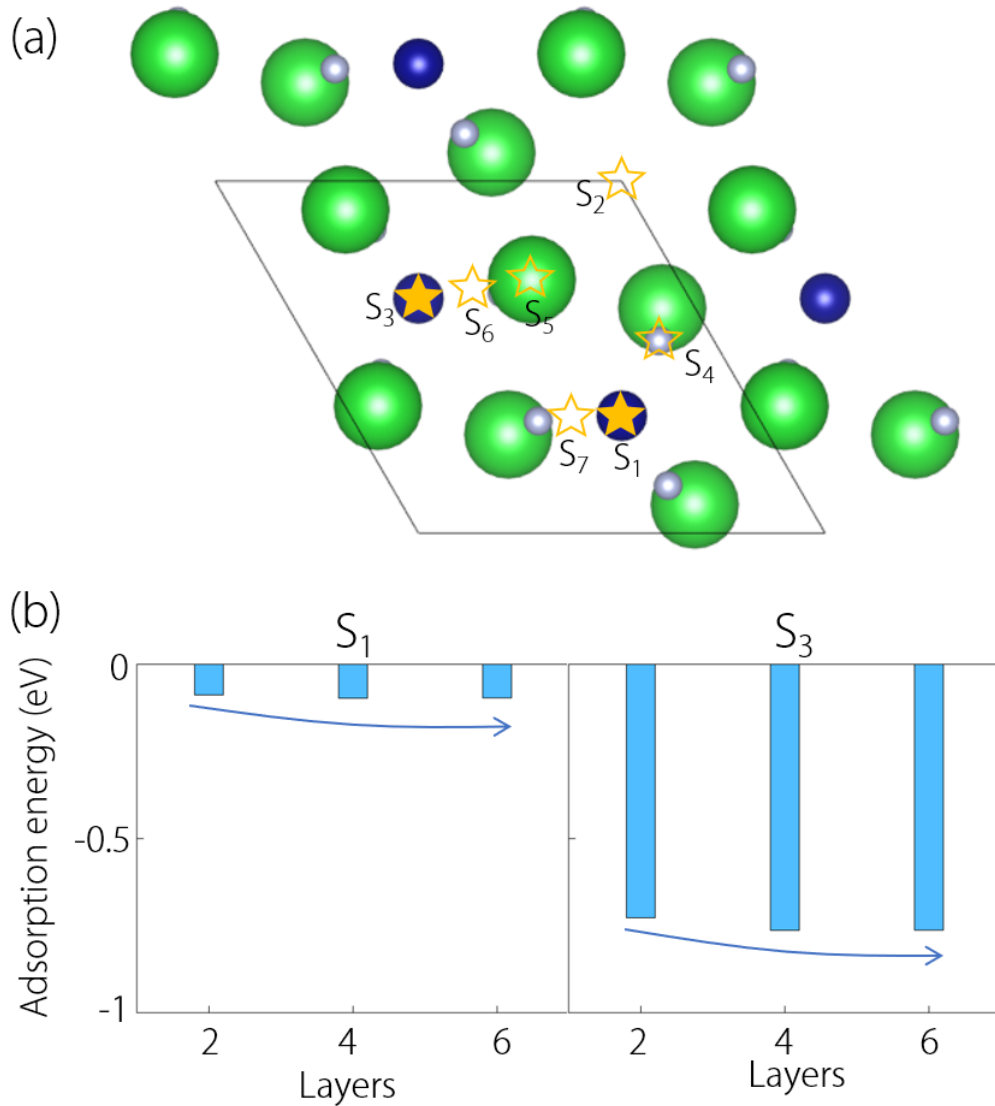


Fig. S3 The energy band with SOC, the inset shows a magnified view of the dashed circle.

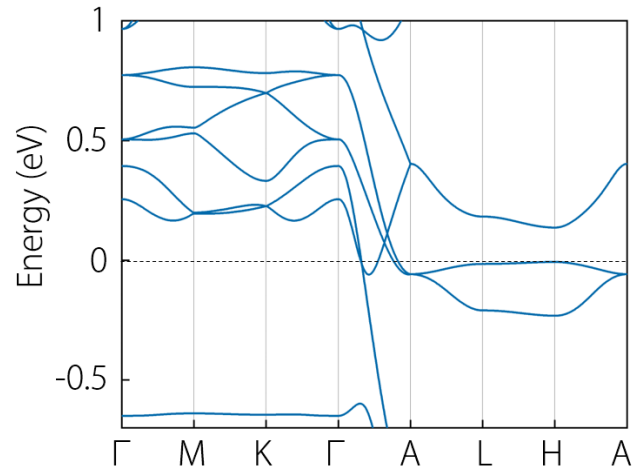
We considered 7 adsorption sites, as shown in Fig. S4a. The solid stars mark stable sites and the hollow stars mark unstable sites. Fig. S4b shows the adsorption energy of S_1 and S_3 sites corresponding to 2, 4 and 6 layers. It can be seen that the adsorption



energy tends to stabilize after 4 layers, while the S_3 site is more stable compared to S_1 .

Fig. S4 (a) Schematic figure of the different sites, where the solid indicate stable sites and the hollow indicate unstable sites. (b) Hydrogen adsorption energies of different layers under adsorption sites S_1 and S_3 , respectively.

We have calculated the band structure of Ba_3CrN_3 after adsorbing H atom (Fig. S5) and found that the topological features are still present, only the energy positions



have changed.

Fig. S5 The band structure after H adsorption.

As shown in Fig. S6, there is no imaginary frequency in the phonon spectra of Ba_3CrN_3 under the largest tensile and compressed strain, demonstrating its dynamical stability under strain. In addition, we also calculated the ab initio molecular dynamics simulation of Ba_3CrN_3 under these strain at 300K, as shown in Fig. S7, indicating its thermal stability under strain.

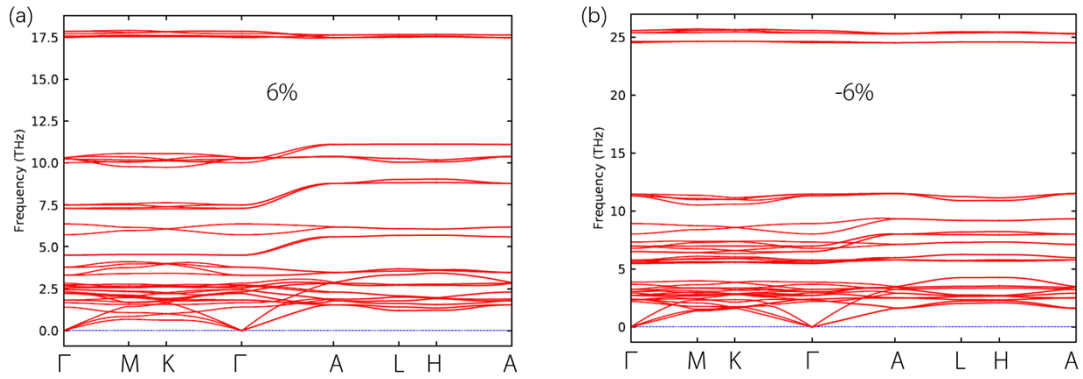


Fig. S6 Calculated phonon spectrum of Ba_3CrN_3 under (a) 6% and (b) -6% strain.

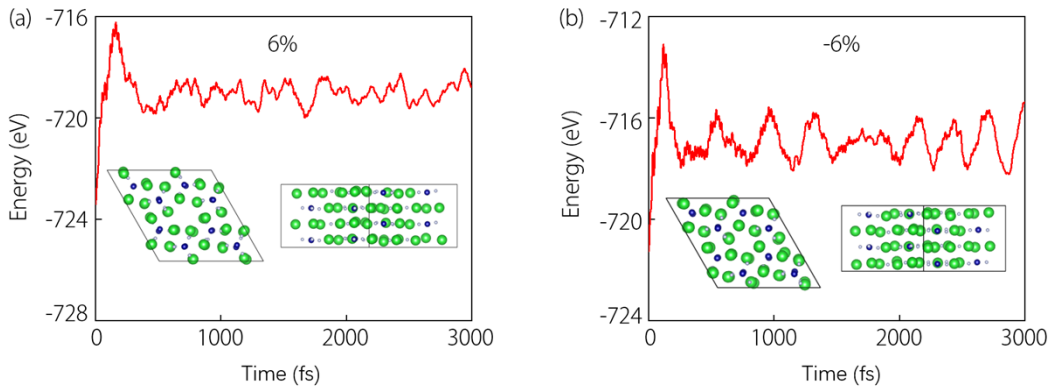


Fig. S7 Calculated AIMD of Ba_3CrN_3 under (a) 6% and (b) -6% strain.

In Fig. S8, we note that all crossing points are preserved when strain is applied. However, P_2 changes to Type-II TP when compressive strain is applied, and Type-I TP when tensile strain is applied. These crossing points move progressively closer to the Fermi level as the strain changes from -6%~6%.

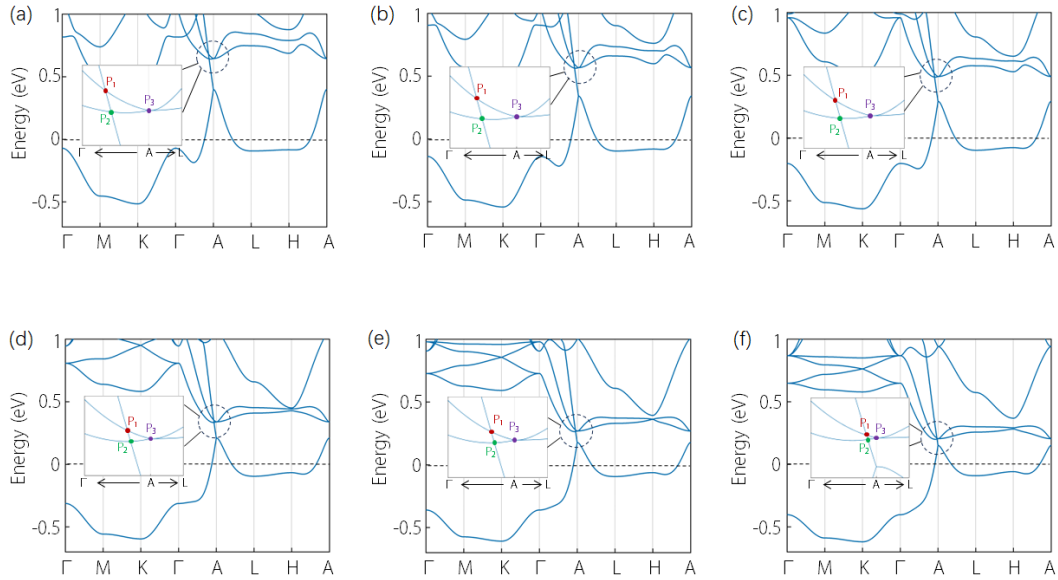


Fig. S8 Energy band structure for Ba₃CrN₃ under biaxial pressure stress (a-c) and tensile stress (d-f). The deformation of lattice from Figure (a) to Figure (f) is -6%, -4%, -2%, 2%, 4%, 6%, the inset shows a magnified view of the dashed circle.

Fig. S9 shows the energy distribution of the nodal surface in $k_z=\pi$ plane, where the red region denotes the high energy region and the blue region denotes the low energy region, and the white arcs represent the intersection line of the nodal surface and the Fermi level, so the area within the white line is the projected area of the nodal surface (PANS) on the Fermi level. It can be seen that the PANS gradually increase when the strain of -6% to 6% is applied.

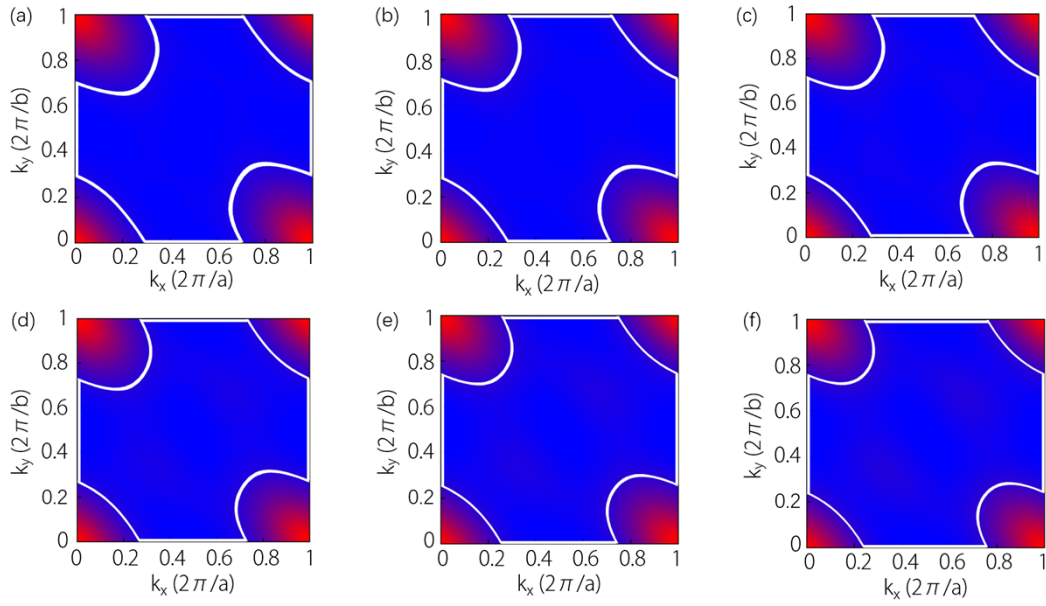


Fig. S9 The energy contour plot of the nodal surface under biaxial pressure stress (a-c) and tensile stress (d-f). The deformation of lattice from Figure (a) to Figure (f) is -6%, -4%, -2%, 2%, 4%, 6%.

Fig. S10 illustrates the band structure of Ba_3CrN_3 when doped with different cavities, and it can be seen that except for the nodal surface, the other crossing points are stable and far away from the Fermi level. We believe that the cause of this phenomenon is that with the doping of cavities, more and more valence band electrons are neutralized, leading to a decrease of the Fermi level.

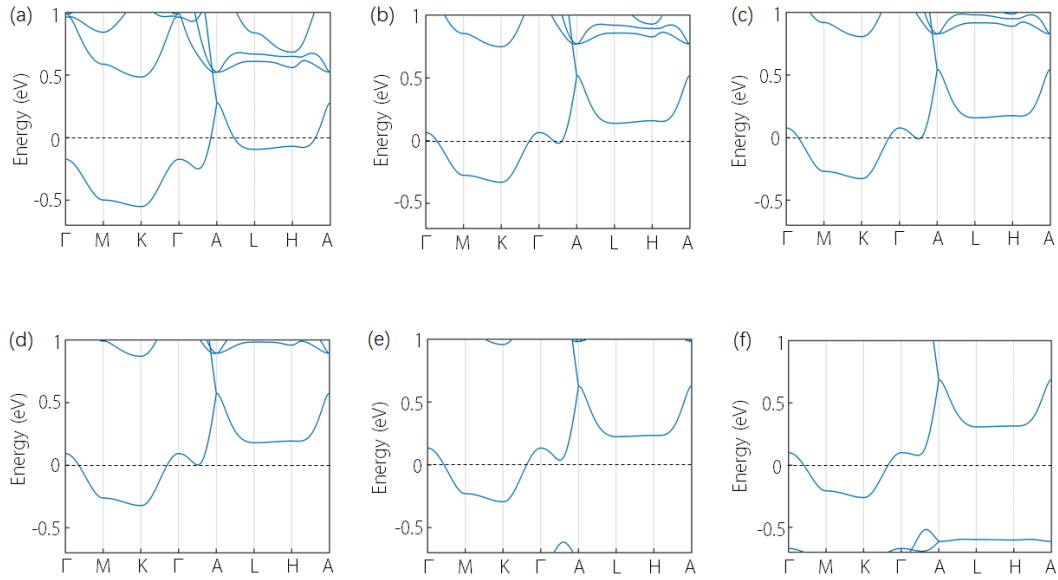


Fig. S10 Energy band structure for Ba_3CrN_3 with doping holes. Here, the number of holes from (a) to (f) is 0, 0.2, 0.4, 0.6, 0.8, 1, respectively.

We tried to break symmetry by rotating the CrN_3 unit with the Cr atom at fractional coordinates $(1/3, 2/3, 1/4)$, as shown in Fig. S11a. In this case, the symmetry is indeed broken (Fig. S11e), but the adsorption energy does not show a large change compared to that when rotating the CrN_3 unit with the Cr atom at fractional coordinates $(2/3, 1/3, 3/4)$. Then we compared the DOS of IE in the two cases (Fig. S11b), and found that the DOS of IE is more stable when rotating the lower CrN_3 unit. We believe that in this case the interstitial electrons will play a major role in the process of H adsorption, and therefore the adsorption energy will also remain stable.

To further verify the role of the nodal surface in H adsorption, we translated the lower CrN_3 unit upwards, as shown in the inset in Fig. S12a. This deformation is also able to destroy the nodal surface (Fig. S12b). In this case, the DOS of IE remains stable, but the adsorption energy is significantly reduced, demonstrating that the nodal surface indeed plays a role in the adsorption process.

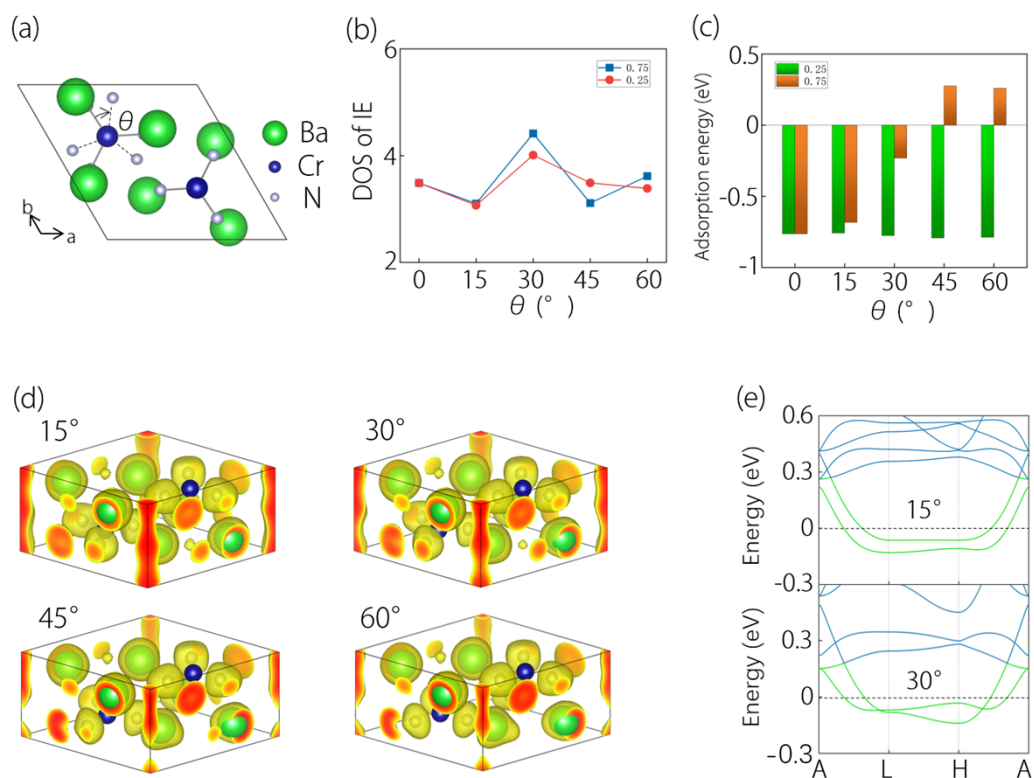


Fig. S11 (a) Schematic illustration for rotating the CrN₃ unit with the Cr atom at fractional coordinates (1/3, 2/3, 1/4). (b) Comparison of DOS of IE corresponding to different rotating angles of CrN₃ units around the Cr atom at (2/3, 1/3, 3/4) and (1/3, 2/3, 1/4). (c) Comparison of adsorption energy corresponding to different rotating angles of CrN₃ units around the Cr atom at (2/3, 1/3, 3/4) and (1/3, 2/3, 1/4). (d) The ELF of rotating 15°, 30°, 45°, 60° in electride Ba₃CrN₃, with the isosurface value set as 0.65. (e) The electronic band structures for rotating 15° and 30°.

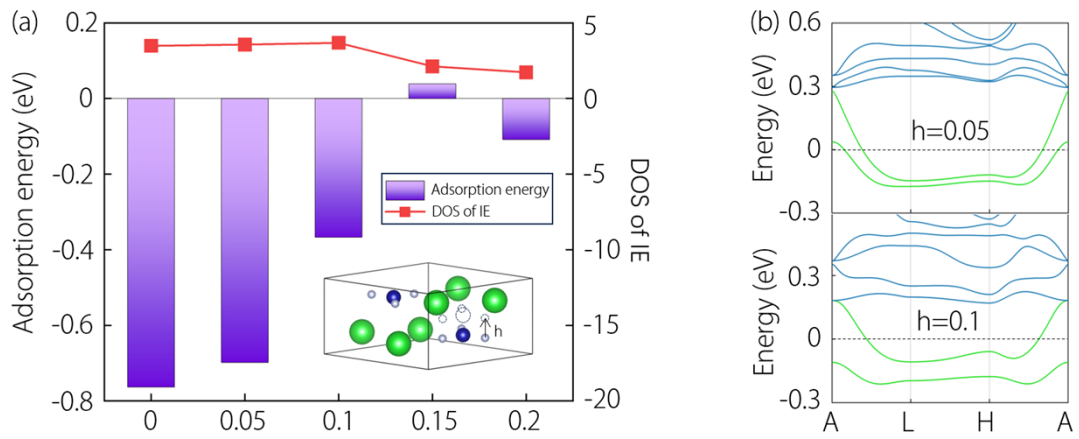


Fig. S12 (a) The adsorption energy and DOS of IE corresponding to different displacement distances of CrN₃ units around the Cr atom at (1/3, 2/3, 1/4). The illustration is the schematic diagram of moving the CrN₃ unit with the Cr atom at fractional coordinates (1/3, 2/3, 1/4). (b) The electronic band structures for moving 0.05 and 0.1.

Supplementary Tables

The adsorption energy of the S_1 and S_3 sites in Figure S4a corresponding to 2,4 and 6 layers are listed in Table S1, where it can be seen that the S_3 site is more stable and the adsorption energy tends to a constant value after 4 layers.

Layer	S_1	S_3
2	-0.08753 eV	-0.72730 eV
4	-0.09765 eV	-0.76346 eV
6	-0.09626 eV	-0.76325 eV

Table S1 Hydrogen adsorption energy of S_1 and S_3 site under different layers.

Table S2 lists the EW, PANS and ΔE_H under strain from -6% to 6%. It can be seen that as the strain changes from -6% to 6%, the EW decreases, the PANS increases, and the ΔE_H remains stable.

Table S2 The EW, PANS and ΔE_H of Ba_3CrN_3 under -6%~6% biaxial strain.

Strain (%)	-6	-4	-2	0	2	4	6
EW (eV)	0.4906	0.4279	0.3892	0.3448	0.3054	0.2710	0.2419
PANS	0.3402	0.3306	0.3208	0.3052	0.2940	0.2668	0.2256
ΔE_H (eV)	-0.683	-0.717	-0.746	-0.763	-0.764	-0.747	-0.714

Table S3 lists the adsorption energy corresponding to doping with 0.2~1 holes. It can be seen that the adsorption energy decreases with increasing hole concentration. And Ba_3CrN_3 loses its adsorption capacity when doped with 0.8 holes.

Table S3 The hydrogen adsorption energy of Ba_3CrN_3 with doping 0.2~1 holes.

Holes	0.2	0.4	0.6	0.8	1.0
ΔE_H (eV)	-0.65547	-0.47197	-0.24658	0.00207	0.26703

We rotated the $[\text{CrN}_3]^{6-}$ unit with the Cr atom at fractional coordinates (2/3, 1/3, 3/4) to break the symmetry in order to disrupt the nodal surface, and Table S4 lists the adsorption energy corresponding to rotations from 0° to 60° , and it can be seen that the adsorption energy decreases as the rotation angle increases, and eventually Ba_3CrN_3 loses the adsorption capacity.

Table S4 The hydrogen adsorption energy of Ba_3CrN_3 when $[\text{CrN}_3]^{6-}$ unit with the Cr atom at fractional coordinates (2/3, 1/3, 3/4) rotates $0\sim 60^\circ$.

θ ($^\circ$)	0	15	30	45	60
ΔE_{H} (eV)	-0.763	-0.683	-0.231	0.275	0.260

In order to further demonstrate the role of the nodal surface in the H adsorption process, we have broken the symmetry by translating the $[\text{CrN}_3]^{6-}$ unit with the Cr atom at fractional coordinates (1/3, 2/3, 1/4) upwards, and the corresponding adsorption energy with different distances of translation are listed in Table S5. It can be seen that the adsorption energy decreases as the translation distance increases, which proves that the nodal surface does play a role in the H adsorption process.

Table S5 The hydrogen adsorption energy of Ba_3CrN_3 when $[\text{CrN}_3]^{6-}$ unit with the Cr atom at fractional coordinates (1/3, 2/3, 1/4) moves 0.05~0.2

h	0	0.05	0.1	0.15	0.2
ΔE_{H} (eV)	-0.763	-0.698	-0.367	0.039	-0.109